# A new Approximate Bayesian Computation framework to distinguish among complex evolutionary models using whole-genome data

Silvia Ghirotto[*§], Maria Teresa Vizzari[*], Francesca Tassi, Guido Barbujani and Andrea Benazzo[§]

Department of Life Sciences and Biotechnology, University of Ferrara, 44121 Ferrara, Italy

[*] these authors contributed equally to this work

[§] correspondence should be addressed to andrea.benazzo@unife.it and silvia.ghirotto@unife.it

## Abstract

Inferring past demographic histories is crucial in population genetics, and the amount of complete genomes now available for many species should in principle facilitate this inference. In practice, however, the available inferential methods suffer from severe limitations. Although hundreds complete genomes can be simultaneously analyzed, complex demographic processes can easily exceed computational constraints, and there are no standard procedures to make sure that the estimates obtained are reliable. Here we present ABC-SeS, a new Approximate Bayesian Computation (ABC) framework, based on the Random Forest algorithm, to infer complex past population processes using complete genomes. All possible pairs of populations are compared, and the data are summarized by the full genomic distribution of the four mutually exclusive categories of segregating sites, a set of statistics fast to compute even from unphased genome data. We constructed an efficient ABC pipeline and tested how accurately it allows one to recognize the true model among models of increasing complexity, using simulated data and taking into account different sampling strategies in terms of number of individuals analyzed, number and size of the genetic loci considered. Once assessed the power of ABC-SeS in the comparison of even complex models, we applied it to the analysis of real data, testing models on the dispersal of anatomically modern humans out of Africa and exploring the evolutionary relationships of the three species of

Orangutan inhabiting Borneo and Sumatra. The flexibility of our ABC framework, combined with the power provided by the set of statistics proposed pave the way for reliable inference of past population processes for any species for which high coverage genomes are available.

## Authors' summary

We propose a new method for inferring demographic history from whole-genome data, ABC-SeS. The idea is to analyze the distributions of segregating sites within an Approximate Bayesian Computation framework, using a Random Forest approach. Extensive simulation shows that ABC-SeS can handle very large datasets and identify the model that generated the data, even when population relationships are complicated by factors such as admixture. We also provide guidelines concerning the sampling strategies leading to the most accurate inference. As examples of possible applications, we show: (1) that complex alternative models on human dispersal out of Africa can now be formally tested and compared by ABC-SeS; and (2) that the evolutionary relationships among three orangutan species can now be better assessed by ABC-SeS than by alternative methods.

## Introduction

A robust reconstruction of the demographic dynamics of a species is important both to improve our knowledge about the past and to disentangle the effects of demography from those of natural selection [1–3]. In recent years, thousands of modern and ancient complete genome sequences have become available, potentially containing vast amounts of information about the evolutionary history of populations [4–10]. However, these genomes do not speak by themselves; to extract the evolutionary information they contain, appropriate inferential statistical methods are required. Some methods based on the Sequential Markovian Coalescent (SMC) model [11], became popular among population geneticists due to their ability to infer population size changes through time (PSMC [12]) and divergence times (MSMC [13]), and to scale well on whole genome

sequences. Under these approaches, the local density of heterozygote sites along chromosomes is used to estimate the times of the most recent common ancestor (TMRCA) of genomic regions separated by recombination, thus providing insight into ancestral population sizes and the timing of past divergence processes. These estimates are often used to indirectly support hypotheses regarding the evolution of the studied organisms. Albeit sophisticated, these methods present some limitations; the temporal resolution of the inferred demographic events seems to be strongly dependent on the number of individuals included, with poor performance in the recent past especially when analyzing single individuals. Moreover, these methods assume no gene flow among the investigated populations, which in many case is plainly implausible. The consequences on the inferential process of violation of this assumption are still under investigation [14].

Other methods infer demographic parameters via the diffusion approximation [15], or coalescent simulations [16], from the site frequency spectrum (SFS) computed on large genomic datasets. The SFS records the observed number of polymorphisms segregating at different frequencies in a sample of *n* individuals and it is generally computed over a certain number of genomic regions where no influence of natural selection is assumed. The expectation of the SFS under different evolutionary scenarios could be approximated by the diffusion theory (as implemented e.g. in *dadi*) or directly via coalescent simulations (as in *fastsimcoal*); alternative demographic histories can be explicitly compared via e.g. AIC [17]. Still, there are limits to the complexity of models that can be analyzed, and AIC-like approaches can only be used to understand which modifications significantly improve the model. Therefore, through these approaches, it is not easy to evaluate whether and to what extent the compared models can actually be distinguished from each other, and hence quantify the strength of the support associated to the best model. Indeed, the only available procedure to assess the model identifiability requires the analysis of many datasets simulated under known demographic conditions, which can be computationally prohibitive, in particular for complex evolutionary scenarios [16].

Recently, an inferential method that couples the ability of the SMC to deal with whole

genome sequences and the population signal gathered from the SFS has been developed (SMC++ [18] ). Under this inferential framework, both the genomic and the SFS variation are jointly used to estimate population size trajectories through time, as well as the divergence time between pairs of populations. Although this approach seems to scale well on thousands of unphased genomes, it is based on the same assumption of classical SMC methods (with populations evolving independently), which severely limits its use whenever gene flow cannot be ruled out.

One powerful and flexible way to quantitatively compare alternative models and estimating model's parameters relies on the Approximate Bayesian Computation (ABC) methods. Under these methods, the likelihood functions do not need be specified, because posterior distributions can be approximated by simulation, even under complex (and hence realistic) population models, incorporating prior information. The genetic data, both observed and simulated, are summarized by the same set of "sufficient" summary statistics, selected to be informative about the genealogic processes under investigation. The ability of the framework to distinguish among the alternative demographic models tested and the quality of the results can be evaluated with rather limited additional effort (for a review see e.g. [19]). Although ABC has the potential to deal with complex and realistic evolutionary scenarios, its application to the analysis of large genomic datasets, such as complete genomes, is still problematic. In its original formulation, indeed, the ABC procedure requires the simulation of millions data sets of the same size of those observed, which becomes computationally very expensive as the dataset increases in size, or when many models need be compared. In addition, there is a problem with the choice of the summary statistics describing both observed and simulated data, as recognized since the first formal introduction of ABC [20,21]. Increasing the number of summary statistics, indeed, makes it easier to choose the best model, but inevitably reduces the accuracy of the demographic inference (this problem is referred to as the "curse of dimensionality" [22]). Ideally, the good practice would be to select a set of summary statistics that is both low-dimensional and highly informative on the demographic parameters defining the model. In practice, however, this problem has never really been solved, despite several

serious attempts [23].

Recently, a new ABC framework has been developed based on a machine-learning tool called Random Forest (ABC-RF [24]). Under ABC-RF, the Bayesian model selection is rephrased as a classification problem. At first, the classifier is constructed from simulations from the prior distribution via a machine learning RF algorithm. Once the classifier is constructed and applied to the observed data, the posterior probability of the resulting model can be approximated through another RF that regresses the selection error over the statistics used to summarize the data. The RF classification algorithm has been shown to be insensitive both to the correlation between the predictors (in case of ABC, the summary statistics) and to the presence of relatively large numbers of noisy variables. This means that even choosing a large collection of summary statistics, the correlation between some of them and others (which may be uninformative about the models tested), have no consequences on the RF performance, and hence on the accuracy of the inference. Moreover, compared to the standard ABC methods, the RF algorithm performs well with a radically lower number of simulations (from millions to tens of thousands per model). These properties make the new ABC-RF algorithm of particular interest for the statistical analysis of massive genetic datasets.

In this paper we present ABC-SeS (where SeS stands for Segregating Sites), a new framework for demographic inference via ABC-RF, suitable for the analysis of complete genomes. ABC-SeS compares all possible pairs of populations, summarizing both the observed and the simulated genetic variation by the distribution over the genome of the four mutually exclusive categories of segregating sites (i.e. private polymorphisms in either population, shared polymorphisms and fixed differences) known to be informative about processes of divergence and admixture [25], and not requiring phased data. These statistics have already been successfully used in a standard ABC context [26], but only in the form of the first four moments of the distribution across loci. Here, for the first time, and thanks to the ABC-RF procedure, we analyze the full genomic distribution of each statistic. We performed a power analysis, to evaluate how accurately

this ABC pipeline can recognize the true model among models of increasing complexity, using simulated data. We also explored the inferential power of the presented procedure with respect to the experimental conditions, evaluating the consequences of sampling strategies involving different numbers of genomes, different numbers of loci, and different locus lengths. Finally, we applied our method to two case studies. First, we analyzed the demographic history of anatomically modern humans and the dynamics of migration out of the African continent, explicitly comparing the models proposed by [27,28]. Secondly, we reconstructed the past demographic history and the interaction dynamics among the three orangutan species inhabiting Borneo and Sumatra, revising the models presented by [29].

# Results

## Summary Statistics

We summarize the genetic data by means of the genomic distributions of the four mutually exclusive categories of segregating sites in two populations, namely 1- segregating sites private of the first population, 2- segregating sites private of the second populations, 3- segregating sites that are polymorphic in both populations and 4- segregating sites fixed for different alleles in both populations [25]. To calculate the complete genomic distribution of these statistics we considered the genome as subdivided in a certain number of independent fragments of a certain length, and for each fragment we counted the number of sites belonging to each of the four above-mentioned categories. The final vector of summary statistics is thus composed by the truncated frequency distribution of fragments having from 0 to *n* segregating sites in each category, for each pair of populations considered. We refer to this set of statistics as FDSS (frequency distribution of segregating sites) hereafter. The maximum number of segregating sites in a locus of a certain length is fixed to *n*, and hence the last category contains all the observations higher than *n*. In the one population models, the four distributions described above collapse in a single distribution describing the frequency of loci showing specific levels of within-population segregating sites.

156

157 **Power Analysis**

158 To determine the power of the ABC-SeS procedure in distinguishing among alternative
159 evolutionary trajectories, we performed an extensive power analysis, as described below.

160 We simulated genetic data considering different experimental conditions, thus testing all the
161 possible combinations of locus length (bp) {200; 500; 1,000; 2,000; 5,000}, number of loci {1,000;
162 5,000; 10,000} and number of chromosomes {2, 4, 10, 20}, for a total of 60 combinations of
163 sampling conditions tested. The data were generated using the *msms* simulator according to each of
164 these combinations for three sets of non-nested models of increasing complexity, namely one-
165 population models (four alternative models, Fig 1A), two-population models (three alternative
166 models, Fig 2A) and multi-populations models (two alternative models, Fig 3A); for a more
167 comprehensive description of the models see the Materials and Methods section.

168 For each combination of experimental conditions, we compared alternative models within
169 the three sets tested treating 1,000 simulated datasets for each model as pseudo-observed data
170 (pods). The models were compared through ABC-RF, and we counted the number of times the
171 model selection procedure correctly assigned a pod to the true model, i.e. to the model that actually
172 generated that pseudo-observed dataset. The proportion of true positives (TP) thus calculated is a
173 measure of the power of the whole procedure, considering all its features (model selection
174 approach, alternative models compared, statistics summarizing the data, genomic parameters
175 simulated). The TP results are summarized in Figs 1-3B.

176

177 *One-population models*

178 We designed four one-population models, respectively considering a population of constant
179 size through time, a bottleneck, an exponential growth and a structured population. In each of the
180 50,000 simulations (per model and per combination of experimental parameters) demographic and
181 evolutionary parameter values are drawn from prior distributions, detailed in S1 Table. The four

plots of Fig 1B report the results of the power analyses. In each plot, we see the proportion of times each model was correctly recognized as the most likely one. In general, the percentage of true positives is quite high, ranging from almost 80% to 100% depending on the model generating the pod and on the combination of experimental conditions tested. The bottleneck model has the highest rate of identification, with most combinations of experimental conditions yielding nearly 100% true positives. By contrast, the least identifiable model seems the one considering a structured population, with 0.76 to 0.86 true positives, depending on the combination of experimental conditions. However, we observed that the decrease in the power is actually linked to the extent of gene flow among demes, and to the number of demes sampled; as increasing gene flow and decreasing the number of demes sampled, the structured and the panmictic models converge, hence becoming harder to distinguish (S2 Fig). As expected, we observed a general increase in the power with the increase of both the locus length and the number of loci considered. The number of sampled chromosomes does not appear to be directly linked to the increase of the proportion of true positives. For some sampling conditions, we observed instead a decrease in the TP rate going from 2 to 20 chromosomes (see Fig 1B). However, we showed that this unexpected behavior can be explained with the overlap of the FDSS generated by the constant and the structured models, which increases as increasing the number of chromosomes sampled (S3 Fig). We repeated the whole analysis considering intra-locus recombination (S4 Fig), and the general pattern did not change. We observed a reduced power for the structured model (TP from 75 to 90%) with respect to the other models tested (TP from 80 to 100%), and a stronger effect of the locus length and of the number of loci, than of the number of chromosomes simulated.

*Two-populations models*

The two-population scenarios include a divergence model with isolation after the divergence (no gene flow); a divergence model with continuous migration from the separation until present times; and a divergence model with a single event of bidirectional migration (i.e. pulse of

admixture), for a total of three models compared for each combination of experimental parameters (Fig 2A, prior distributions reported in S2 Table). The plots in Fig 2B clearly show that the most recognizable model is the one including divergence and migration, with proportions of true positives close to 0.95, regardless of the combination of experimental conditions tested. For the other two models, the power was clearly lower than that estimated for the one-population models, with values ranging from 40% to 65% (for the model without migration) and from 60% to 80% (for the model with a pulse of admixture). This low power might be due to the fact that, when the pulse of admixture of the third model occurs right after the divergence, the two models become essentially identical. To verify this prediction, we calculated the proportion of TP for the pulse of admixture model, subdividing the pods in seven categories, depending on the time interval between the divergence and the admixture event (S5 Fig). The proportion of the pods correctly assigned to the pulse of admixture model increases as the intervals between divergence and admixture increase, reaching values of 85% for some combination of parameters. In this case, we did not observe remarkable differences with respect to specific experimental parameters. The performance of the method improved when we included intra-locus recombination in the simulations (S6 Fig). In this case, we observed an increase of the power with increasing locus length, both for the no migration and for the pulse of admixture model, respectively reaching values of 95% and 100%.

We also ran many parallel simulations, using either the whole FDSS or its first four moments only. In all cases (a selection of the results is in S3 Table) the FDSS's ability to distinguish among different evolutionary scenarios was greater, and sometimes substantially so, under the former conditions.

*Multi-populations models*

In most realistic cases, interactions among several populations need be considered. Among the many possible scenarios, we chose to initially focus on the alternative hypotheses proposed to explain the expansion of anatomically modern humans out of the African continent. We shall refer

to the two models (shown in Fig 3A and detailed in Materials and Methods) as Single Dispersal (proposed e.g. in [27]) and the Multiple Dispersal (proposed e.g. in [28,30,31]). The main demographic events are shared between the two models, and here we shall refer to the description given by [27]: three archaic branches (unknown, Denisova and Neandertal), three modern branches (Africans, Eurasians and Papuans) and a specific pattern of gene flow. The difference between the two alternative models lies in the details of the expansion from Africa. Under the Single Dispersal model (SDM), Eurasians and Papuans derived from the same expansion from Africa, through the Near East. Under the Multiple Dispersal model (MDM), the Papuans derived from an earlier dispersal from Africa, independent from that giving rise to the Eurasian populations.

The prior distributions associated with these models are reported in S4 and S5 Table. Fig 3B summarizes the power analysis. The proportion of true positives ranges between 0.65 and 0.70 for the SDM, regardless of the combination of experimental parameters tested, and between 0.6 and 0.8 for the MDM, in this case with a slight increase of the power with the size of the fragments simulated. Being the SDM and the MDM quite similar, in particular when the time interval between the first and second exit in the MDM is short, we also evaluated the ABC-SeS ability to identify the correct model as a function of the time span between the divergence time of the African ghost populations and the second exit in the Multiple Dispersal model. To do this, we considered 10,000 pods from the MDM. We then subdivided these 10,000 pods in 6 bins of increasing interval between these two events (up to 60,000 years), and, within each bin, we separately calculated the proportion of times in which the MDM is correctly recognized by the ABC-RF procedure. As might be expected, the proportion of true positives increases with increasing intervals between the divergence of the two African ghost populations and the time of the second exit (S7 Fig), reaching values of 90% for some combinations of experimental parameters.

For the multi-populations models we tested the effect of intra-locus recombination only for 4 key sampling schemes that combine few (1,000) and many (10,000) genetic loci with either short (500 bp) or long (2,000 bp) DNA fragments. We selected these combinations because they might

represent extremely favorable (10,000 loci, 2,000 bp length) or unfavorable (1,000 loci 500bp length) conditions that can be encountered when analyzing real data. Compared with the results obtained for the same experimental parameters without considering intra-locus recombination, we observed a slight increase in the TP rate when analyzing high number of fragments, or when considering longer locus lengths (S6 Table).

**Real Case: out of Africa dynamics**

Simulations in the previous section basically show that alternative models can be distinguished by ABC-SeS, except when they differ for parameters approaching 0, thus creating overlaps between their expected consequences. We then moved to applying the ABC-SeS method to estimate posterior probabilities of alternative models about early human expansion from Africa. Whether human demographic history is better understood assuming one [5,27] or two [28,30,31] major episodes of African dispersal is still an open question. While concluding that indigenous Australians and Papuans seem to derive their ancestry from the same African wave of dispersal as most Eurasians, Mallick et al. [5] admitted that these inferences change depending on the computational method used for phasing haplotypes. Therefore, it made sense to compare the SDM and the MDM by ABC-SeS. For this purpose, we analyzed the high coverage Neandertal genome [7], the high coverage Denisova genome [6], and a large set of modern individuals published in [28] (S7 Table). To make sure that the choice of the genomes does not affect the results, we repeated the model selection analysis replacing the Papuan individuals with those published by [27] (S7 Table). We extracted from all these genomes 10,000 shared independent fragments of 500 base pairs length (see Material and Methods for details). Since we knew that the number of chromosomes has a minor impact on the analysis, we considered two chromosomes per population, so that the sample size would be the same in ancient and modern samples. The proportion of true positives for the combination of experimental parameters here considered (i.e. 10,000 loci of 500 bp length and 2 chromosomes per population) was 0.66 for the SDM, and between 0.69 and 0.85 for the MDM (Fig

3A and S7 Fig). Considering recombination, we observed an increase of the proportion of TP for the MDM, which (averaged over the whole range of possible divergence times between the African ghost populations and the second exit) reached a value of 0.75.

As the SDM and the MDM mainly differ for the origin of the Papuan population (whether or not descending from the same ancestor of Eurasians), to test for the robustness of the results we used the genomic information of all the six Papuan individuals sequenced by [28]. To this purpose, we repeated the ABC-RF model selection procedure six times, each time considering a different Papuan individual. Fig 4 and S8-S11 Tables presents the results of the ABC-RF model selection, showing that, in all the comparisons, the results supported the MDM, with posterior probabilities ranging from 0.67 to 0.69. We repeated the whole analysis considering the 25 Papuan individuals in [27], this time repeating the ABC-RF model selection procedure 25 times, and always found results favoring the MDM over the SDM. The posterior probabilities estimated for the MDM were comparable to those estimated with the Pagani dataset [28] (Fig 4). Considering intra-locus recombination, MDM received additional support, with posterior probabilities ranging from 0.70 to 0.76 for both datasets (Fig 4).

**Real Case: Orangutan evolutionary history**

As a second application of our framework to real data, we investigated the past demographic and evolutionary dynamics of the three known orangutan species. In addition to the orangutan species previously recognized in Borneo (*Pongo pygmeus*) and in Sumatra, North of Lake Toba (*Pongo abelii*), [29] described a new species of Sumatran orangutan, *Pongo tapanuliensis*, South of Lake Toba. To reduce the otherwise excessive computational effort in their ABC analysis, [29] had to compare simplified versions of the alternative models. Factors such as bottlenecks and population structure were considered only when estimating the parameters of the best-performing model, namely the one with an earlier split between the two Sumatran species, and an origin of the Bornean species from *Pongo tapanuliensis* ancestors. The ABC-SeS method does not suffer from this

shortcoming. We compared four complex scenarios, designed following the models presented in [29] (Fig 5A). While considering the same substructure within the three orangutan species, the four models differ in the genealogical relationships assumed among species (Fig 5A and Materials and Methods for details). From the whole genomic dataset presented in [29], we selected seven individuals, one from each of the populations emerged from the study (S12 Table, see Materials and Methods for details). Following the procedure described in Materials and Methods, we extracted 9,000 independent sites 1kb length shared among the 7 selected individuals, on which we calculated the FDSS. We generated 50,000 simulations per model considering the above mentioned genomic structure (9,000 loci, 1kb length and 2 chromosomes per population), with prior distributions detailed in S13-S16 Tables. We first assessed the ability to correctly recognize the four alternative models tested through a power analysis, considering 1,000 pods per model. The results are presented in Fig 5A. The most identifiable model (TP=0.81) appeared to be the model 2b, under which there is a first separation of South Toba from Borneo Orangutan, followed by the divergence of North Toba from South Toba. The model assuming an early separation of South Toba form North Toba, followed by the separation of Borneo from South Toba, actually showed the lowest proportion of true positives (0.45). The application to real data favored the model 1a, (also associated with the highest posterior probability in [29]), with a posterior probability of 0.49. Under the most supported model both the North Toba (first) and Borneo (later) separated from *Pongo tapanuliensis* Fig 5B.

## Discussion

The cost of typing large genomic datasets has dramatically decreased lately, making population-scale genomic data available for a large set of organisms [4,9,10,32,33]. The main challenge now is how to extract as much information as possible from these data, developing flexible and robust statistical methods of analysis [12,13,16]. Approximate Bayesian Computation, explicitly comparing alternative demographic models and estimating the models' probabilities,

represents a powerful inferential tool for about past population dynamics [34]. Another advantage of such a simulation-based approach is the possibility to easily check whether the models being compared are actually distinguishable, hence quantifying the reliability of the estimates produced [35]. Nevertheless, only recently, with the development of the Random Forest procedure for ABC model selection [24], it has become possible to apply ABC to large genomic datasets. With this work, we took advantage of this newly proposed algorithm to develop ABC-SeS, an ABC-based flexible framework to compare demographic models. The novelty of this framework mainly lies in the summary statistics used to summarize genomic data, namely the complete genomic distribution of the four mutually exclusive categories of segregating sites for pairs of populations [25].

**Power Analysis**

Initially, we analyzed sets of models with increasing levels of complexity, simulating genetic data under a broad spectrum of experimental conditions. This extensive power analysis showed that ABC-SeS can often identify the model under which the data were generated, with some uncertainties only when two models are just marginally different. This was the case for both simple (one or two-population scenarios, Figs 1 and 2) and complex (multi-populations scenarios, Fig 3) demographies. When we compared one-population scenarios, to summarize the data we necessarily considered only one of the four distributions of polymorphic sites. Nonetheless the model identifiability, calculated as the proportion on TPs over 1,000 pods, reached values between 80% and 100%, with slightly lower values only for the structured model. This reduction in the power was always due to the levels of gene flow among demes; when it is high, the structured model becomes hardly distinguishable from the panmictic model (S2 Fig), as has already been known since Wright's times [36]. We also showed that the power depends on the number of demes; indeed, the proportion of TPs increases in parallel with the number of demes considered in the structured model (S2 Fig). Among the two-populations demographies, the model with bi-directional migration at a constant rate proved easiest to identify, with almost 100% TPs, regardless of the combination of

364 experimental parameters tested. Predictably (see e.g. [37]), the pulse of admixture model produced
365 the most accurate results when the two populations were highly genetically divergent and the time
366 interval between admixture and divergence was large (S5 Fig). Our results showed that models are
367 difficult to discriminate only when the divergence is recent, and/or close the admixture event. Pods
368 generated under these conditions, indeed, are often erroneously assigned to the other models.

369 Even when more complicated scenarios were compared (e.g., the multi-populations models),
370 the ABC-SeS framework recognizes the true model, with about 70% TPs. It is worth noting that in
371 the MDM the first and the second exit from Africa could sometimes occur at very close times. In
372 these cases, the SDM and the MDM models become extremely similar. Indeed, we observed an
373 increase in the power of the test at increasing intervals between the African divergence and the
374 second exit (S7 Fig), reaching values close to 90%.

375 In the first round of comparisons, we assumed complete linkage among all sites within the
376 same fragment. Even if acceptable for some experimental conditions (i.e. for short locus lengths),
377 this is generally simplistic. We thus repeated the power tests, this time generating data that could
378 undergo intra-locus recombination. In all the comparisons, we found that, with recombination, the
379 results are generally better, regardless of the experimental parameters considered, and particularly
380 when the loci are long. In particular, we observed a substantial increase of the proportion of TPs for
381 the MDM, but not for the SDM (S6 Table). One possible explanation for this finding is, in a tree
382 generated under SDM, all loci of the African, European, Asian and Papuan populations, belong to a
383 branch that has a unique topology (T1 in S8 Fig) and recombination will not alter this condition. By
384 contrast, under MDM, the topologies are three (T1, T2 and T3 in S8 Fig) a recombination event will
385 generate a transition from one of these baseline topologies to the recombinant topology (denoted as
386 R in S8 Fig). Thus, recombination under MDM reduces the fraction of loci showing the T1
387 topology, i.e. the topology shared with the alternative SDM, thus increasing the possibility that the
388 two models be discriminated. As could be expected, under most conditions tested, the model
389 identifiability increases increasing the locus length, and the number of loci considered. Indeed, by

analyzing more loci and longer loci, the probability of observing recombination increases, resulting in a higher fraction of the R topologies. Thus, when one is analyzing many loci, or long stretches of DNA, recombination should be considered, although this is not necessarily leading to an increase in TPs, because the specific features of the demographic models compared are also a factor.

As it is intuitively reasonable, and how it has been already pointed out e.g. by [38], the accuracy of the model selection seems to be more dependent on the number of loci considered and on the locus length rather than on the number of individuals sampled per population. In absence of recombination, the locus length appeared to be crucial to correctly identify simple demographies, such as those generated under one-population models, whereas its effect was minor when complex scenarios were compared (Figs 1 and 3). When recombination was included in the modeling, the locus length seemed to become the main factor leading to a good discrimination between models. In the two-populations scenarios we observed a significant increase of the proportion of TPs at increasing lengths of the fragments simulated, reaching values close to 100% (S6 Fig). It is anyway worth noting that the power to correctly identify the true model was quite good even when we simulated short fragments, as well as in the comparison of complex demographies (Fig 3). This finding means that the ABC-SeS procedure is particularly suitable for the analysis of ancient data [6] and of RAD sequencing data [39], where short DNA fragments are more the rule than the exception.

**Applications to real datasets**

We compared two demographic models about the anatomically modern humans expansion out of Africa, combining ancient (Neandertal and Denisova) and modern genomes data. Because we were including ancient data, we restricted the analysis to short fragments (500 bp) to maximize the number of independent loci retrievable. This combination of experimental parameters (10,000 loci 500 bp length, 2 chromosomes per population) showed anyway a good ability to distinguish between models (Fig 3). For the first comparison, we used as modern genomes those published by

[28], and repeated the model selection procedure six time, each time considering one of the six Papuan genomes in the dataset. All such comparisons supported the MDM (Fig 4), i.e. a first expansion of the ancestors of the current Austro-Melanesians, followed by a second expansion leading to the peopling of Eurasia. We obtained the same conclusion by using Papuan genomes coming from another dataset [27] (Fig 4). Considering different modern individuals from African, European and Asian populations did not change the support for the MDM. These results raise several questions; indeed, it was the SDM that showed the best fit in [27], whereas the MDM appeared to account for the data only when the analysis was restricted to modern populations. However, our findings are in agreement with those by [28], who estimated that at least 2% of the Papuan genome derive from an earlier, and distinct, dispersal out of Africa. Other genomic studies [31], but not all [5], and phenotypic analyses [30] appear support the MDM, which calls for further research in this area. Be that as it may, in no other study besides the present one (i) the alternative hypotheses are explicitly compared analyzing complete genomes; (ii) posterior probabilities are estimated for each model, and (iii) the accuracy of the estimates is assessed by power analysis.

We then moved to investigating the evolutionary history of the three extant Orangutan subspecies, the last of which (located south of the Lake Toba) has been recently described by [29]. We basically repeated the ABC analysis performed by [29] applying our ABC-SeS framework. Nater and colleagues [29] started comparing simple evolutionary scenarios, and considered population substructure and gene flow only when estimating parameters, but not in the phase of model choice. ABC-SeS allowed us to analyze complex demographies from the very beginning, i.e. from the model selection phase, thus comparing more realistic evolutionary scenarios. We basically obtained the same results presented by [29]; in both cases the most supported model was the one accounting for a first separation of the North Toba and a later separation of the Borneo species from the newly identified South Toba species (Fig 5B). The main difference was about the strength of the support associated to this model. While Nater and colleagues [29] estimated high posterior probabilities for the best-fitting model (73% when comparing the 4 models and 98% when

comparing the two best scenarios), our procedure associated to the same model a posterior probability of 49% (Fig 5A). Moreover, the power analysis that we conducted (absent in [29]), revealed that the ability to correctly distinguish among the four tested models is between 45% and 81%, with the selected model that can be erroneously recognized as the most probable one in the 38% of cases. These results emphasize (i) the importance of including complex demographic histories in the model selection step, so as to evaluate the real posterior probability associated to the best model, on which the parameter estimation will be performed and (ii) the importance of performing a power analysis of the models tested, so as to be aware of the level of uncertainty about the conclusions of the study.

**Perspectives**

In this paper we presented a new framework based on ABC-RF to explicitly compare complex demographic models exploiting whole-genome data. We proposed to summarize the data with a set of statistics that were already known to be informative about past population dynamics [25], but for the first time, and thanks to the Random Forest algorithm, we used the entire genomic distribution of the four categories of segregating sites between pairs of populations in an ABC context. It is clear that considering the whole FDSS, rather than its first four moments, significantly improves our ability to distinguish among different evolutionary scenarios. How large this improvement, depends on the amount of genetic loci available, and, of course, on how large are the differences between the alternative models. At present, the ABC-SeS is optimized for high-coverage genotypes [5,10,33]. A natural extension of this work will thus be to implement the use of low coverage data, developing an approach able to retrieve the FDSS taking into account the genotype uncertainty and sequencing errors, for instance through the use of the genotype likelihood (as, e.g., in ANGSD [40]).

The flexibility of the ABC-RF model selection approach, combined with the inferential power proven by the summary statistics that we proposed to calculate on genomic data, pave the

way for a detailed and comprehensive study of complex demographic dynamics for any species for which few high coverage genomes are available.

# Materials and Methods

## ABC Random Forest

Approximate Bayesian computation is a flexible framework, based on coalescent simulations, to compare different evolutionary hypotheses and identify the one that with the highest probability generated the observed data [20,34]. Despite its potential, the application of the classical ABC approach to the analysis of large genomic datasets and complex evolutionary models, has been quite limited. Possible reasons are (i) the levels of arbitrarity in the choice of the sufficient set of summary statistics and (ii) the high number of simulations required to obtain good quality posterior estimates, resulting in an unacceptable increase of computational time when multiple complex models are simultaneously analyzed. Both these issues appear to have been solved with the development of a new ABC approach, based on a machine learning procedure (Random Forest [24]). Random Forest uses the simulated datasets for each model in a reference table to predict the best fitting model at each possible value of a set of covariates. After selecting it, another Random Forest obtained from regressing the probability of error of the same covariates estimates the posterior probability. This procedure allows one to overcome the difficulties traditionally associated with the choice of summary statistics, while gaining a larger discrimination power among the competing models. Moreover, a satisfying level of accuracy in the estimates is achieved with about 30-50 thousand simulations per model [24], significantly reducing the computational cost of the analysis of complex demographic histories. All the ABC-RF estimates have been obtained using the function *abcrf* from the package abcrf and employing a forest of 500 trees, a number suggested to provide the best trade-off between computational efficiency and statistical precision [24]. We compared all models and obtained the posterior probabilities using the function *predict* from the same package.

494

495 **Power Analysis**

496 For the power analysis, we generated data under different combinations of experimental
497 parameters, varying the number of loci (calculating FDSS on 1,000, 5,000 and 10,000 loci), the
498 locus length (200; 500; 1,000; 2,000; 5,000 bp) and the number of chromosomes sampled per
499 population (2, 4, 10, 20), for a total of 60 combinations per model. We evaluated the power
500 considering three sets of models of increasing complexity, detailed below.

501

502 **One-population models.**

503 We started by considering four demographic models (Fig 1). The first model represents a
504 constantly evolving population with an effective population size *N1*, drawn from a uniform prior
505 distribution (S1 Table). Under the second model, the population experienced a bottleneck of
506 intensity *i*, *T* generations ago. The intensity and the time of the bottleneck, and the ancient effective
507 population size *Na* are drawn from uniform prior distributions, showed in S1 Table. The third
508 model represents an expanding population. The expansion (of intensity *i*) is exponential and starts *T*
509 generations ago, with the effective population size increasing from *N1/i* to *N1* (prior distributions in
510 S1 Table). Under the last model, the population is structured in different demes, exchanging
511 migrants at a certain rate. The actual number of demes *d*, the migration rate *m* and the effective
512 population size *N1* are drawn from prior distributions (S1 Table).

513 **Two-populations models.**

514 We then moved to considering three demographic models with two populations (Fig 2). The
515 first one is a simple split model without gene flow after the divergence. Under this model, an
516 ancestral population of size *Nanc* splits *Tsep* generation ago into two populations. These two
517 derived populations evolve with a constant population size (*N1* and *N2*) until the present time
518 (priors for these free parameters are shown in S2 Table). The second model also includes a
519 continuous and bidirectional migration, all the way from the divergence moment to the present. The

per generation migration rates *m12* and *m21* are drawn from priors defined in S2 Table. The third and last model assumes a single pulse of bidirectional admixture at time *Tadm* after divergence. Admixture rates *adm12 adm21*, and the time of admixture are drawn from priors (S2 Table).

**Multi-populations models.**

Finally, we compared two demographic models, representing the two alternative hypotheses that have been proposed to explain the dispersal of anatomically modern humans out of the African continent (i.e single and multiple dispersals, Fig 3). To design the models we followed the parametrization proposed by [27], with some minor modifications. Both models share the main demographic structure: on the left the archaic groups (i.e. Neandertal, Denisova and an unknown archaic source), and on the right the anatomically modern humans (with a first separation between Africans and non-Africans and subsequent separations among population that left Africa). Given the evidence for admixture of Neandertals and Denisovans with non-African modern human populations [6,7], we allowed for genetic exchanges from archaic to modern species, indicated in Fig 3 by the colored arrows. It has to be noted that the archaic populations actually sending migrants to modern humans are two ghost populations that diverged from the Denisovan and the Neandertal Altai samples 393 kya and 110 kya, respectively [27]. This way, we took into account that the archaic contributions to the modern gene pool did not necessarily come from the archaic populations that have been genotyped so far. We modeled bidirectional migration between modern populations along a stepping-stone, thus allowing for gene flow only between geographically neighboring populations. Under the Single Dispersal model (SDM) a single wave of migration outside Africa gave rise to both Eurasian and Austromelanesian populations, whereas under the Multiple Dispersal model (MDM) there are two waves of migration out of Africa, the first giving rise to Austromelanesians and the second to Eurasians. We took into account the presence of genetic structure within Africa modeling the expansion from a single unsampled "ghost" population under the SD model, and from two separated unsampled "ghost" populations for the MD model. The prior distributions for all the parameters considered in these models are in S4 and S5 Tables.

We simulated both demographic models under all possible combinations of experimental parameters. We ran 50,000 simulations per model and combination of experimental parameters, using the *ms/msms* software [41,42]. To evaluate the quality of the estimates of the model selection procedure we calculated the proportion of True Positives (TP) as follows. We randomly sampled 1,000 datasets from each simulated combination of demographic model and experimental parameters. We treated each of these sampled datasets as pseudo-observed data (pod) and performed a models comparison within the correspondent set of models tested. For each model and combination of experimental parameters, we calculated the proportion of TPs as the proportion of times the true model was the most supported by the model selection procedure.

## Real Case: out of Africa dynamics

We considered the ancient high-coverage genomes of Denisova and Neandertal [6,7], together with modern human samples from [28]. A detailed description of the samples is in S7 Table. All the individuals were mapped against the human reference genome hg19 build 37. To calculate the observed FDSS we only considered autosomal regions found outside known and predicted genes +/- 10,000 bp and outside CpG islands and repeated regions (as defined on the UCSC platform, [43]). We also took into consideration only the fragments found in genomic regions that passed a set of minimal quality filters used for the analysis of the ancient genomes (map35_50%, [6,7]). From the resulting regions we extracted 10,000 independent fragments of 500 bp length, separated by at least 10,000 bps. All comparisons involved a single individual (i.e. two chromosomes) per population, and so each run of the analysis took into account the Denisova, the Neandertal, one African, one European one Asian and one Papuan individual (detailed in S7 Table). We calculated the observed FDSS six times, each time considering a different Papuan individual present in the Pagani dataset [28]. We repeated the whole procedure substituting the Papuan individuals with those published by [27]. To do this, we downloaded the corresponding alignments in CRAM format from https://www.ebi.ac.uk/ega/datasets/EGAD00001001634. The *mpileup* and

572 *call* commands from *samtools-1.6* [44], were used to call all variants within the 10,000 neutral
573 genomic fragments, using the *--consensus-caller* flag, without considering indels. We then filtered
574 the initial call set according to the filters reported in [27] using *vcflib* and *bcftools* [44]. We
575 calculated the FDSS for each of these Papuan individuals, hence obtaining 25 observed FDSS, that
576 have been separately analyzed through the ABC-RF model selection procedure.
577
578 **Real Case: Orangutan evolutionary history**
579 We selected seven Orangutan individuals, one from each of the populations defined by [29],
580 choosing the genomes presenting the highest coverage (S12 Table). We downloaded the FASTQ
581 files from https://www.ncbi.nlm.nih.gov/sra/PRJEB19688, and mapped the reads to the ponAbe2
582 reference genome (http://genome.wustl.edu/genomes/detail/pongo-abelii/) using the BWA-MEM
583 v0.7.15) [45]. We used picard-tools-1.98 (http://picard.sourceforge.net/) to add read groups and to
584 filtered out duplicated reads from the BAM aligments. We performed local realignment around
585 indels by the Genome Analysis Toolkit (GATK) v2.7-2 [46]. To obtain genomic fragments suitable
586 to calculate the FDSS, we generated a mappability mask (identified with the *GEM-mappability*
587 module from the *GEM* library build [47]) so as to consider only genomic positions within a
588 uniquely mappable 100-mer (up to 4 mismatches allowed). We then excluded from this mask all the
589 exonic regions +/- 10,000 bp, repeated regions (as defined in the *Pongo abelii* Ensembl gene
590 annotation release 78), as well as loci on the X chromosome and in the mitochondrial genome. We
591 then generated the final mask calculating the number of fragments separated by at least 10 kb, thus
592 obtaining 9,000 fragments of 1,000 bp length. We called the SNPs within these fragments using the
593 *UnifiedGenotyper* algorithm from *GATK*; the filtering step has been performed as reported in [29]
594 through *vcflib*. We finally calculated the observed FDSS from the quality filtered VCF file.
595 To investigate past population dynamics of the three Orangutan species, we designed
596 competitive scenarios following the demographic models reported in [29]. Nater [29] first compared
597 models assuming simple demographies, and then estimated the parameters from a more complicated

598 model. By contrast, we directly compared complex demographies, designing the within-species
599 substructure as described by [29], (Fig 5A). The four competing models indeed share the same
600 within species features (four populations for the Bornean group, two Sumatran populations north of
601 Lake Toba, and a single population south of Lake Toba), while differing for the topology, i.e. for
602 the evolutionary relationships among the three species, as reported in Fig 5A. We modeled
603 bidirectional migration both among populations within a species and between neighboring species.
604 A detailed description of the models' parameters and of the priors are in S13-S16 Tables. We ran
605 50,000 simulations per model using the *ms* software [41], generating two chromosomes per
606 population (4 Bornean, 1 south of Lake Toba and 2 north of Lake Toba), and 9,000 independent
607 fragments of 1kb length per chromosome. We first assessed the power to distinguish among the four
608 models calculating the proportion of TPs as described above, and then explicitly compared the
609 simulated variation with the FDSS calculated on the observed data (Fig 5B).
610

611 ## Software and data availability

612 All the scripts of the ABC-SeS framework can be found at https://github.com/anbena/ABC-SeS.
613

614 ## Acknowledgments

615 We would like to thank the DFG Center for Advanced Studies, ''Words, Bones, Genes, Tools,'' at
616 University of Tübingen, that hosted AB and SG during the first phase of the project. FT was
617 supported by ERC Advanced Grant 295733, 'LanGeLin'.
618

619 ## Author Contributions

620 AB conceived the study; AB and SG designed the experiments; MTV, AB, SG and FT analyzed the
621 data; SG, MTV, FT, GB and AB discussed the results; SG, GB and AB wrote the paper with inputs
622 from all coauthors.

623

624 ## References

625 1. Akey JM, Eberle MA, Rieder MJ, Carlson CS, Shriver MD, Nickerson DA, et al. Population
626 history and natural selection shape patterns of genetic variation in 132 genes. PLoS Biol.
627 2004;
628 2. Meyer D, Single RM, Mack SJ, Erlich HA, Thomson G. Signatures of demographic history
629 and natural selection in the human major histocompatibility complex loci. Genetics. 2006;
630 3. Lohmueller KE. The Impact of Population Demography and Selection on the Genetic
631 Architecture of Complex Traits. PLoS Genet. 2014;
632 4. 1000 Genomes Project Consortium. An integrated map of genetic variation. Nature. 2012;
633 5. Mallick S, Li H, Lipson M, Mathieson I, Gymrek M, Racimo F, et al. The Simons Genome
634 Diversity Project: 300 genomes from 142 diverse populations. Nature. 2016;
635 6. Meyer M, Kircher M, Gansauge MT, Li H, Racimo F, Mallick S, et al. A high-coverage
636 genome sequence from an archaic Denisovan individual. Science (80- ). 2012;
637 7. Prüfer K, Racimo F, Patterson N, Jay F, Sankararaman S, Sawyer S, et al. The complete
638 genome sequence of a Neanderthal from the Altai Mountains. Nature. 2014;
639 8. Moreno-Mayar JV, Vinner L, de Barros Damgaard P, de la Fuente C, Chan J, Spence JP, et
640 al. Early human dispersals within the Americas. Science (80- ) [Internet]. 2018 Dec
641 7;362(6419):eaav2621. Available from:
642 http://science.sciencemag.org/content/362/6419/eaav2621.abstract
643 9. Dasmahapatra KK, Walters JR, Briscoe AD, Davey JW, Whibley A, Nadeau NJ, et al.
644 Butterfly genome reveals promiscuous exchange of mimicry adaptations among species.
645 Nature. 2012;
646 10. De Manuel M, Kuhlwilm M, Frandsen P, Sousa VC, Desai T, Prado-Martinez J, et al.
647 Chimpanzee genomic diversity reveals ancient admixture with bonobos. Science (80- ).
648 2016;

649 11. McVean GAT, Cardin NJ. Approximating the coalescent with recombination. Philos Trans R
650 Soc B Biol Sci. 2005;
651 12. Li H, Durbin R. Inference of human population history from individual whole-genome
652 sequences. Nature. 2011;
653 13. Schiffels S, Durbin R. Inferring human population size and separation history from multiple
654 genome sequences. Nat Genet. 2014;
655 14. Heller R, Chikhi L, Siegismund HR. The Confounding Effect of Population Structure on
656 Bayesian Skyline Plot Inferences of Demographic History. PLoS One. 2013;
657 15. Gutenkunst RN, Hernandez RD, Williamson SH, Bustamante CD. Diffusion Approximations
658 for Demographic Inference : DaDi. Nat Preced. 2010;
659 16. Excoffier L, Dupanloup I, Huerta-Sánchez E, Sousa VC, Foll M. Robust Demographic
660 Inference from Genomic and SNP Data. PLoS Genet. 2013;
661 17. Akaike H. A New Look at the Statistical Model Identification. IEEE Trans Automat Contr.
662 1974;
663 18. Terhorst J, Kamm JA, Song YS. Robust and scalable inference of population history from
664 hundreds of unphased whole genomes. Nat Genet. 2017;
665 19. Bertorelle G, Benazzo A, Mona S. ABC as a flexible framework to estimate demography
666 over space and time: Some cons, many pros. Molecular Ecology. 2010.
667 20. Beaumont MA, Zhang W, Balding DJ. Approximate Bayesian computation in population
668 genetics. Genetics. 2002;
669 21. Marjoram P, Molitor J, Plagnol V, Tavare S. Markov chain Monte Carlo without likelihoods.
670 Proc Natl Acad Sci. 2003;
671 22. Blum MGB, François O. Non-linear regression models for Approximate Bayesian
672 Computation. Stat Comput. 2010;
673 23. Blum MGB, Nunes MA, Prangle D, Sisson SA. A Comparative Review of Dimension
674 Reduction Methods in Approximate Bayesian Computation. Stat Sci. 2013;

675 24. Pudlo P, Marin JM, Estoup A, Cornuet JM, Gautier M, Robert CP. Reliable ABC model
676 choice via random forests. Bioinformatics. 2015;
677 25. Wakeley J, Hey J. Estimating ancestral population parameters. Genetics. 1997;
678 26. Robinson JD, Bunnefeld L, Hearn J, Stone GN, Hickerson MJ. ABC inference of multi-
679 population divergence with admixture from unphased population genomic data. Mol Ecol.
680 2014;
681 27. Malaspinas AS, Westaway MC, Muller C, Sousa VC, Lao O, Alves I, et al. A genomic
682 history of Aboriginal Australia. Nature. 2016.
683 28. Pagani L, Lawson DJ, Jagoda E, Mörseburg A, Eriksson A, Mitt M, et al. Genomic analyses
684 inform on migration events during the peopling of Eurasia. Nature. 2016;
685 29. Nater A, Mattle-Greminger MP, Nurcahyo A, Nowak MG, de Manuel M, Desai T, et al.
686 Morphometric, Behavioral, and Genomic Evidence for a New Orangutan Species. Curr Biol.
687 2017;
688 30. Reyes-Centeno H, Ghirotto S, Detroit F, Grimaud-Herve D, Barbujani G, Harvati K.
689 Genomic and cranial phenotype data support multiple modern human dispersals from Africa
690 and a southern route into Asia. Proc Natl Acad Sci. 2014;
691 31. Tassi F, Ghirotto S, Mezzavilla M, Vilaça ST, De Santi L, Barbujani G. Early modern human
692 dispersal from Africa: Genomic evidence for multiple waves of migration. Investig Genet.
693 2015;
694 32. Benazzo A, Trucchi E, Cahill JA, Maisano Delser P, Mona S, Fumagalli M, et al. Survival
695 and divergence in a small group: The extraordinary genomic history of the endangered
696 Apennine brown bear stragglers. Proc Natl Acad Sci. 2017;
697 33. Miller W, Schuster SC, Welch AJ, Ratan A, Bedoya-Reina OC, Zhao F, et al. Polar and
698 brown bear genomes reveal ancient admixture and demographic footprints of past climate
699 change. Proc Natl Acad Sci. 2012;
700 34. Beaumont MA. Approximate Bayesian Computation in Evolution and Ecology. Annu Rev

Ecol Evol Syst. 2010;

35. Csilléry K, Blum MGB, Gaggiotti OE, François O. Approximate Bayesian Computation (ABC) in practice. Trends in Ecology and Evolution. 2010.

36. Wright S. Evolution in Mendelian Populations. Genetics [Internet]. 1931 Mar;16(2):97–159. Available from: https://www.ncbi.nlm.nih.gov/pubmed/17246615

37. Medina P, Thornlow B, Nielsen R, Corbett-Detig R. Estimating the timing of multiple admixture pulses during local ancestry inference. Genetics. 2018;

38. Felsenstein J. Accuracy of coalescent likelihood estimates: Do we need more sites, more sequences, or more loci? Mol Biol Evol. 2006;

39. Rowe HC, Renaut S, Guggisberg A. RAD in the realm of next-generation sequencing technologies. Molecular Ecology. 2011.

40. Korneliussen TS, Albrechtsen A, Nielsen R. ANGSD: Analysis of Next Generation Sequencing Data. BMC Bioinformatics. 2014;

41. Hudson RR. ms: a Program for Generating Samples Under Neutral Models. Bioinformatics. 2002;

42. Ewing G, Hermisson J. MSMS: A coalescent simulation program including recombination, demographic structure and selection at a single locus. Bioinformatics. 2010;

43. Hinrichs AS, Raney BJ, Speir ML, Rhead B, Casper J, Karolchik D, et al. UCSC Data Integrator and Variant Annotation Integrator. Bioinformatics. 2016;

44. Li H, Handsaker B, Wysoker A, Fennell T, Ruan J, Homer N, et al. The Sequence Alignment/Map format and SAMtools. Bioinformatics. 2009;

45. Li H, Durbin R. Fast and accurate long-read alignment with Burrows-Wheeler transform. Bioinformatics. 2010;

46. Van der Auwera GA, Carneiro MO, Hartl C, Poplin R, del Angel G, Levy-Moonshine A, et al. From fastQ data to high-confidence variant calls: The genome analysis toolkit best practices pipeline. Curr Protoc Bioinforma. 2013;

47. Derrien T, Estellé J, Sola SM, Knowles DG, Raineri E, Guigó R, et al. Fast computation and applications of genome mappability. PLoS One. 2012;

## Figures Legend:

**Fig 1. One-population models and proportion of True Positives.** A) Demographic models compared: Constant, Bottleneck, Expansion, Structured population. $N_1$ is the effective population size, *i* the intensity of the bottleneck or of the expansion, *T* the time of the bottleneck or of the start of the expansion, *m* is the migration rate. B) True Positives rates. The plot below each of the four models represents the proportion of TPs obtained analyzing pods coming from the above model under 60 combinations of experimental parameters. Different locus lengths are in the x-axes, number of loci is represented by different colors and the number of chromosomes is represented by different symbols.

**Fig 2. Two-populations models and proportion of True Positives.** A) Demographic models compared: Divergence with isolation, Divergence with migration, Divergence with a single pulse of admixture. $N_{anc}$ is the effective population size of the ancestral population, $N_1$ and $N_2$ are the effective population sizes of the diverged populations, $T_{sep}$ is the time of the split, $m_{12}$ and $m_{21}$ the migration rates, $T_{adm}$ is the time of the single pulse of admixture, $adm_{12}$ and $adm_{21}$ the proportions of admixture. B) True Positives rates. The plots have the same features of Fig 1.

**Fig 3. Multi-populations models and proportion of True Positives.** A) Demographic models compared: Single Dispersal and Multiple Dispersals. The populations sampled are indicated in bold. B) True Positives rates. The plots have the same features of Fig 1.

**Fig 4. Posterior Probabilities for the MDM.** Left panel: posterior probabilities obtained analyzing 6 Papuan individuals from [28], simulating data without (PWR) or considering (PR) intra-locus

753 recombination. Right panel: posterior probabilities obtained analyzing 25 Papuan individuals from
754 [27], simulating data without (MWR) or considering (MR) intra-locus recombination.
755
756 **Fig 5. Demographic models tested to study the evolutionary history of Orangutan species**. A-
757 Four demographic models compared. The numbers in the black boxes indicate the proportion of TP
758 calculated analyzing 1,000 pods coming from that demographic model. NT, Sumatran populations
759 north of Lake Toba; ST, the Sumatran population south of Lake Toba; BO, Bornean populations. B-
760 Number of votes associated to each model by ABC-RF and posterior probability of the most
761 supported model (model 1a).
762

## 763 Supporting Informations

764 **Supplementary Figures:**

765 **S1 Fig. Example of a frequency distribution of segregating sites.** On the x-axes: the number of
766 segregating sites (here from 0 to 20). On the y-axes: the number of genomic loci showing a certain
767 number of segregating sites. We calculated four FDSS for each pair of populations compared
768 (representing the genomic distribution of segregating sites private of the first population, private of
769 the second population, shared, and fixed for different alleles). In the one-population models we used
770 a single FDSS.
771

772 **S2 Fig. Proportion of True positives for the one-population structured model as a function of**
773 **the migration rate (A) and the number of demes considered (B).** (A) Each plot represents the
774 proportion of pods from the structured model assigned to each of the four one-population models
775 with the migration rates among demes in the structured model constrained at ranges of increasing
776 values (from $1*10^{-5}$ to $1*10^{-1}$). All the plots consider two chromosomes and a specific combination
777 of locus length and number of loci; the number of demes in the structured model is fixed to four. In
778 general, the TP rate (in dark blue) decreases as increasing the migration rate among demes, with the

779 constant model erroneously recognize as the true model for higher migration rates. (B) Proportion
780 of pods from the structured model assigned to each of the four one-population models as a function
781 of the number of demes (from 2 to 10). The TP rate increase with the number of demes, regardless
782 of the level of migration among demes.
783
784 **S3 Fig. FDSS generated under the one-population models for each number of chromosomes**
785 **tested.** Each plot represents the FDSS simulated under each of the four one-population models
786 considering 1,000 fragments of 1,000 base pair length, for a specific number of chromosomes
787 sampled. Going from two to twenty chromosomes, we observe an increase of the overlapping
788 between the FDSS generated under the Constant and the Structured model, thus possibly explaining
789 the decrease in the models' identifiability as increasing the number of chromosomes considered.
790
791 **S4 Fig. Proportion of True Positives for the one-population models with recombination.** The
792 plots have the same features of Fig 1, we considered a per nucleotide per generation recombination
793 rate of $1*10^{-8.}$
794
795 **S5 Fig. Proportion of True Positives for the Pulse of Admixture model as a function of the**
796 **time span between the divergence and the admixture.** We expressed the x-axes as $(T_{sep}-$
797 $T_{adm})/T_{sep}$, so as to normalize the results respect to the age of the divergence. Each plot represents
798 the results for a different locus length.
799
800 **S6 Fig. Proportion of True Positives for the two-population models with recombination.** The
801 plots have the same features of Fig 1, we considered a per nucleotide per generation recombination
802 rate of $1*10^{-8}$
803
804 **S7 Fig. Proportion of True Positives for the MDM a function of the time span between the**

805 **divergence time of the African ghost populations and the second exit (Delta tdYG-OOA2).** The
806 time difference between the divergence time of the African ghost populations and the second exit
807 from Africa is on the x-axes and it is expressed in years (considering a generation time of 29 years).
808 Each plot reports the results for a different locus length.
809
810 **S8 Fig. Expected topologies under the SDM and MDM.** T1, T2 and T3 are baseline topologies,
811 of which T1 is shared between SDM and MDM, whereas T2 and T3 are exclusively originated by
812 MDM. R is the recombinant topology expected under MDM.
813
814 **Supplementary Tables:**
815 **S1 Table. Demographic parameters and prior distributions of one-population models.**
816 Mutation and Recombination rates are expressed per nucleotide per generation.
817
818 **S2 Table. Demographic parameters and prior distributions of two-population models.**
819 Mutation and Recombination rates are expressed per nucleotide per generation. Time is in
820 generations.
821
822 **S3 Table. RF Prior Error Rates using the complete FDSS or its first four moments.** We
823 calculated the Prior Error Rates under the complete SDFF and under a summary of the distribution
824 (i.e. the first four moments). We analyzed ten combinations of experimental parameters (indicated
825 in the "ID" column), comparing the three two-population divergence models. ll= locus length, nl=
826 number of loci, r= recombination rate, nc= number of chromosomes. The Prior Error Rate is a
827 measure of the global quality of the RF classifier (the lower the better), which depends on the
828 summary statistics used. The complete FDSS always generate lower values of Prior Error Rates.
829
830 **S4 Table. Demographic parameters and prior distributions of multi-population models:**

**Single Dispersal model.** Migration and admixture rates are expressed per generation, times in years. We considered a generation time of 29 years as in [27]. Per nucleotide per generation mutation and recombination rates are fixed as in [27].

**S5 Table. Demographic parameters and prior distributions of multi-population models: Multiple Dispersals model.** Migration and admixture rates are expressed per generation, times in years. We considered a generation time of 29 years as in [27]. Per nucleotide per generation mutation and recombination rates are fixed as in [27].

**S6 Table. Power Analysis of the Multi-Populations models. Comparison of the results with and without intra-locus recombination for the four combinations of experimental parameters tested.** The first four rows present the results without considering intra-locus recombination, whereas the last four rows refer to the same combinations of experimental parameters simulated considering a per nucleotide per generation recombination rate of $1.12*10^{-8}$. TP% columns represent the percentage of True Positives calculated analyzing 1,000 pods coming from SDM and MDM. SDM mpp and MDM mpp represent the mean posterior probability value obtained for the datasets that have been correctly assigned to the true model.

**S7 Table. Genomes used for the comparison of SDM and MDM using real data.**

**S8 Table. Model selection results using Papuan individuals from [28] without intra-locus recombination.** The first column represents the id of the Papuan sample used in that comparison as reported in the dataset. The second column shows the model selected by the ABC-SeS procedure. The third and the fourth columns represent the proportion of votes assigned to SDM and MDM by the RF algorithm. The last column is the posterior probability of the most supported model.

**S9 Table. Model selection results using Papuan individuals from [28] considering intra-locus recombination.** The first column represents the id of the Papuan sample used in that comparison as reported in the dataset. The second column shows the model selected by the ABC-SeS procedure. The third and the fourth columns represent the proportion of votes assigned to SDM and MDM by the RF algorithm. The last column is the posterior probability of the most supported model.

**S10 Table. Model selection results using Papuan individuals from [27] without intra-locus recombination.** The first column represents the id of the Papuan sample used in that comparison as reported in the dataset. The second column shows the model selected by the ABC-SeS procedure. The third and the fourth columns represent the proportion of votes assigned to SDM and MDM by the RF algorithm. The last column is the posterior probability of the most supported model.

**S11 Table. Model selection results using Papuan individuals from [27] considering intra-locus recombination.** The first column represents the id of the Papuan sample used in that comparison as reported in the dataset. The second column shows the model selected by the ABC-SeS procedure. The third and the fourth columns represent the proportion of votes assigned to SDM and MDM by the RF algorithm. The last column is the posterior probability of the most supported model.

**S12 Table. Genomes used for the comparison of the four Orangutan evolutionary scenarios.**

**S13 Table. Demographic parameters and prior distributions for Model 1a.** Migration rates are expressed per generation, times in years. We used a generation time of 25 years as in [29]. The per nucleotide per generation mutation rate is fixed as in [29].

**S14 Table. Demographic parameters and prior distributions for Model 2a.** Migration rates are expressed per generation, times in years. We used a generation time of 25 years as in [29]. The per

883 nucleotide per generation mutation rate is fixed as in [29].

884

885 **S15 Table. Demographic parameters and prior distributions for Model 1b.** Migration rates are
886 expressed per generation, times in years. We used a generation time of 25 years as in [29]. The per
887 nucleotide per generation mutation rate is fixed as in [29].

888

889 **S16 Table. Demographic parameters and prior distributions for Model 2b.** Migration rates are
890 expressed per generation, times in years. We used a generation time of 25 years as in [29]. The per
891 nucleotide per generation mutation rate is fixed as in [29].

892

A

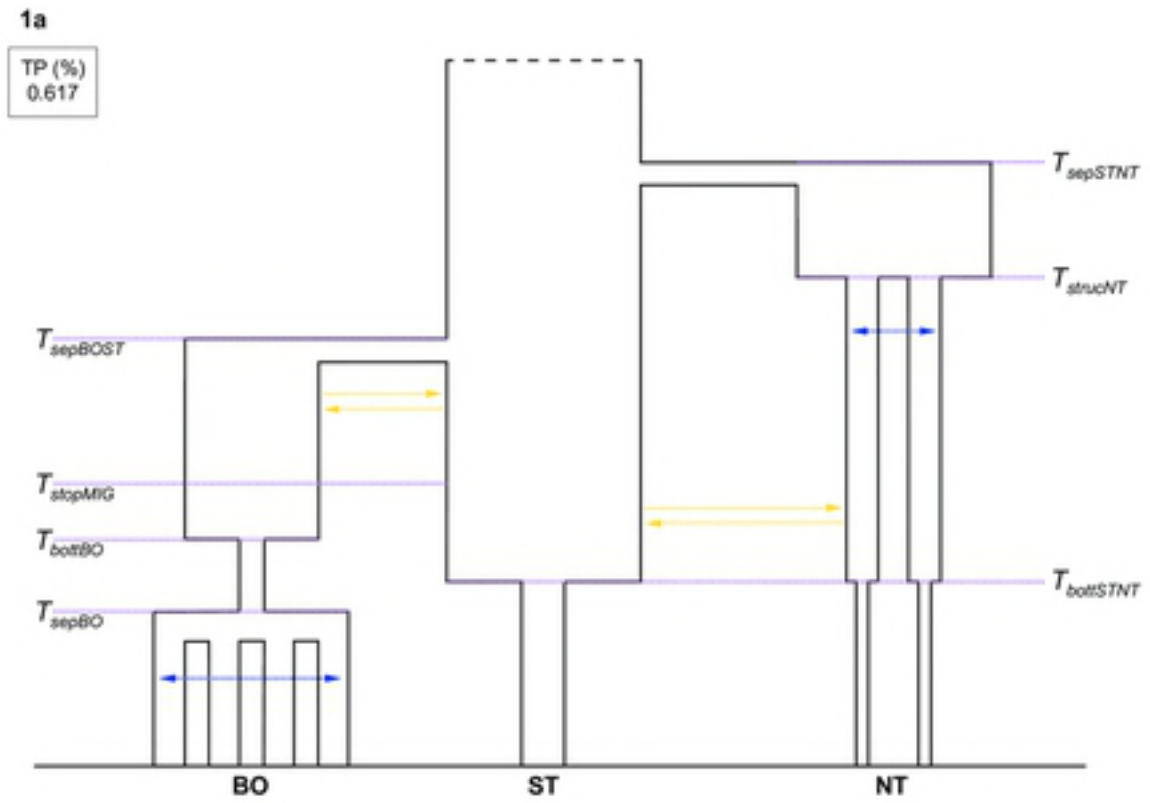


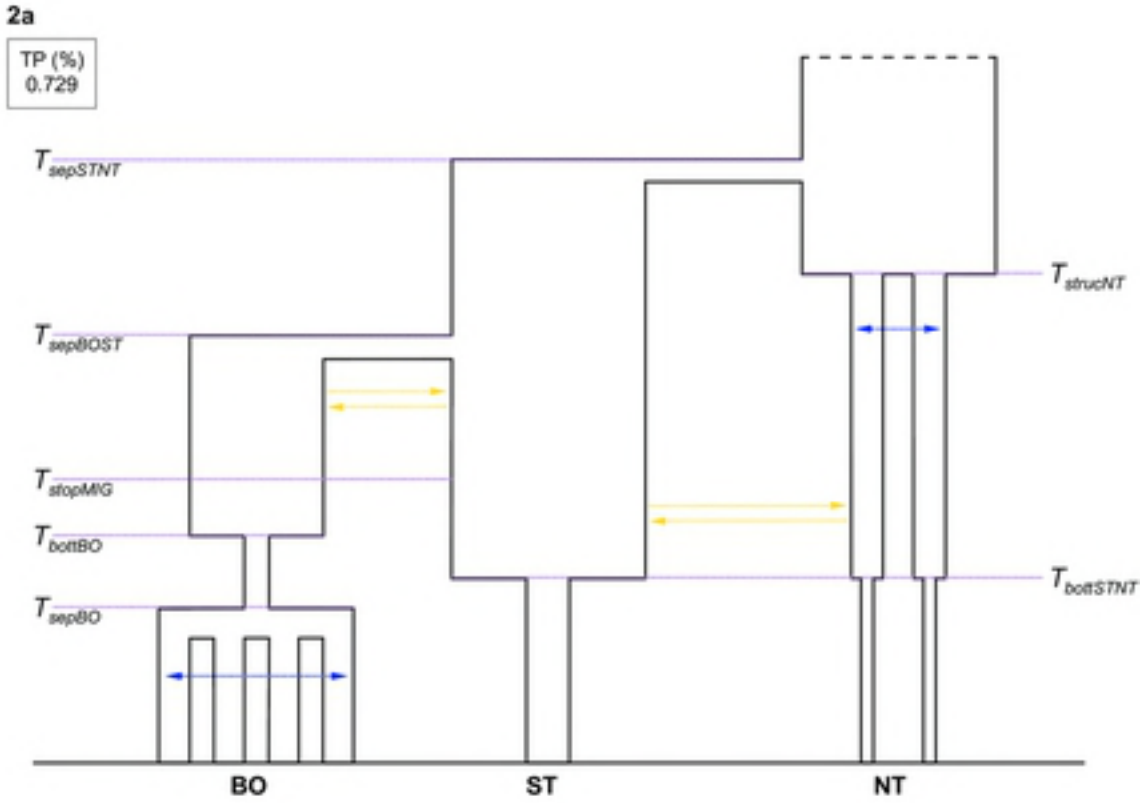


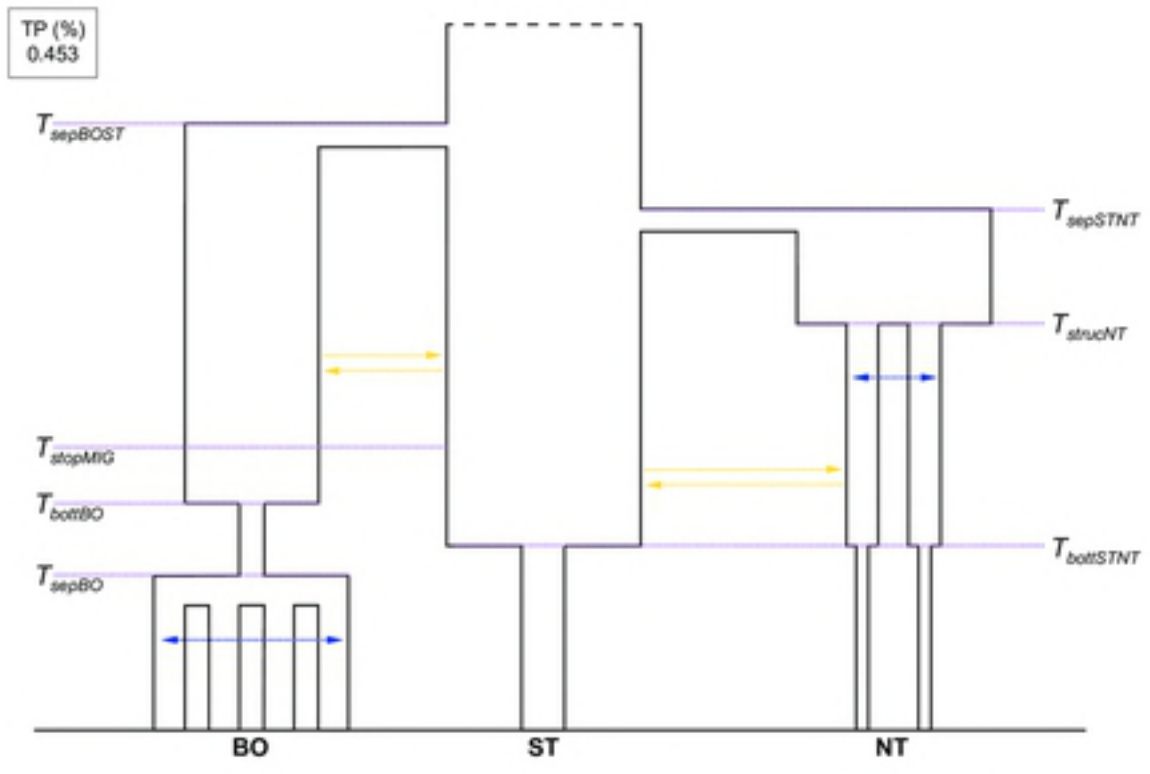


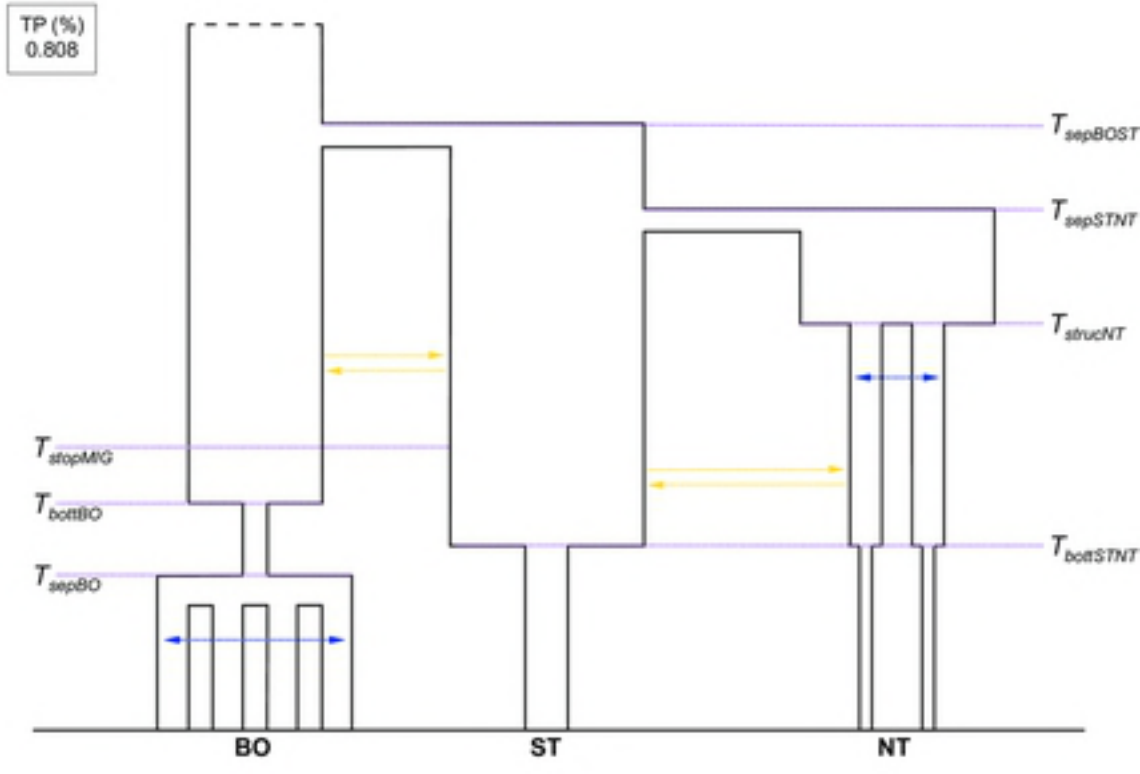


B

| Selected Model | Votes model 1A | Votes model 2A | Votes model 1B | Votes model 2B | PP |
|---|---|---|---|---|---|
| 1A | 0.398 | 0.190 | 0.292 | 0.120 | 0.489 |

Figure 5

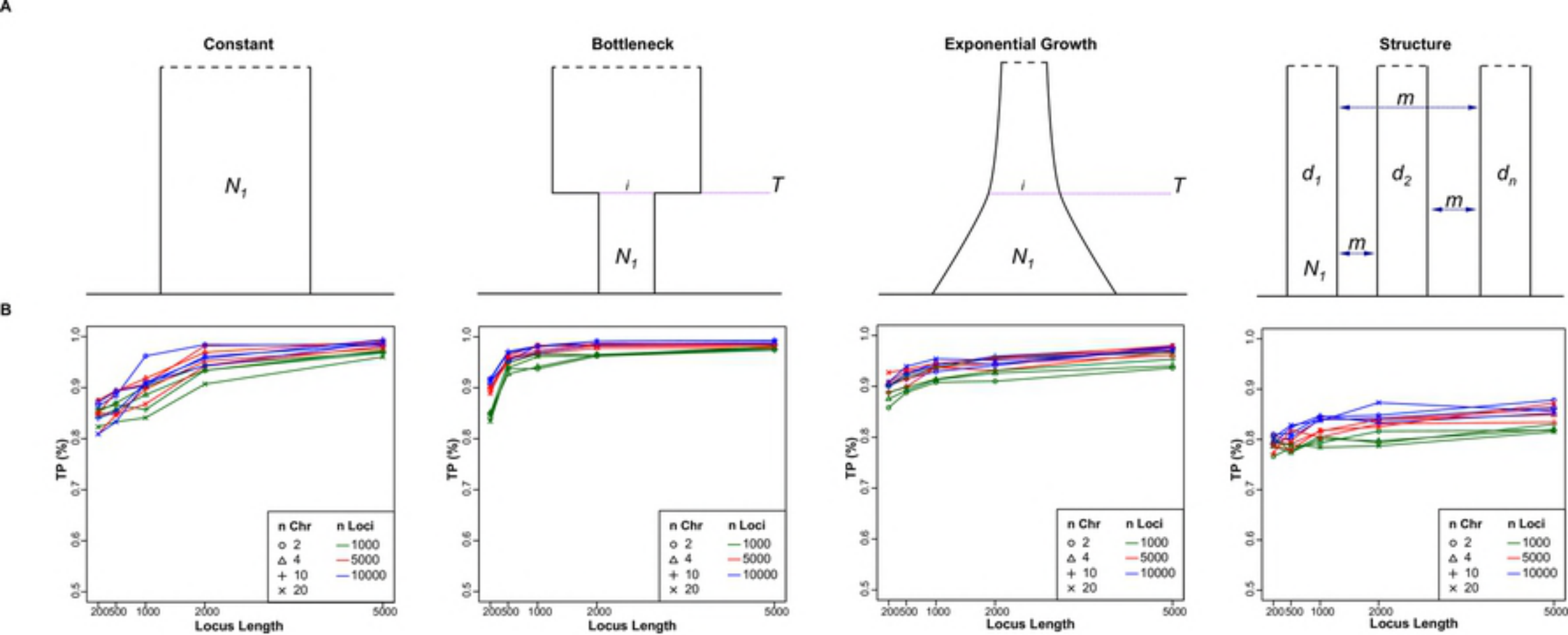
A
Constant
Bottleneck
Exponential Growth
Structure
$N_1$
$i$
$T$
$m$
$d_1$
$d_2$
$d_n$
B
TP (%)
Locus Length
n Chr
n Loci
2
4
10
20
1000
5000
10000

Figure 1

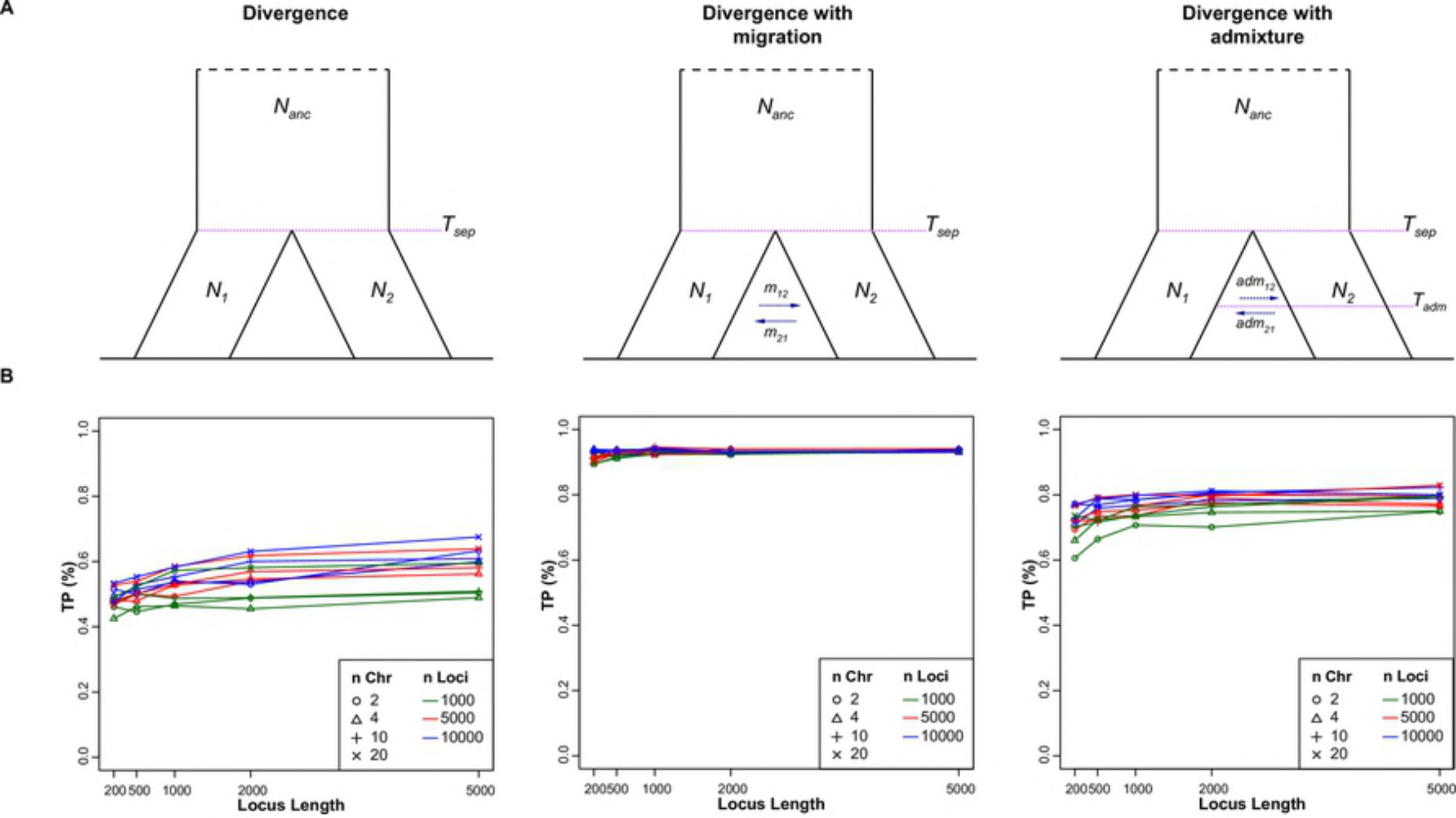
A
Divergence
Divergence with migration
Divergence with admixture
$N_{anc}$
$T_{sep}$
$N_1$
$N_2$
$m_{12}$
$m_{21}$
$adm_{12}$
$adm_{21}$
$T_{adm}$
B
TP (%)
Locus Length
n Chr
n Loci
2
4
10
20
1000
5000
10000

Figure 2

A

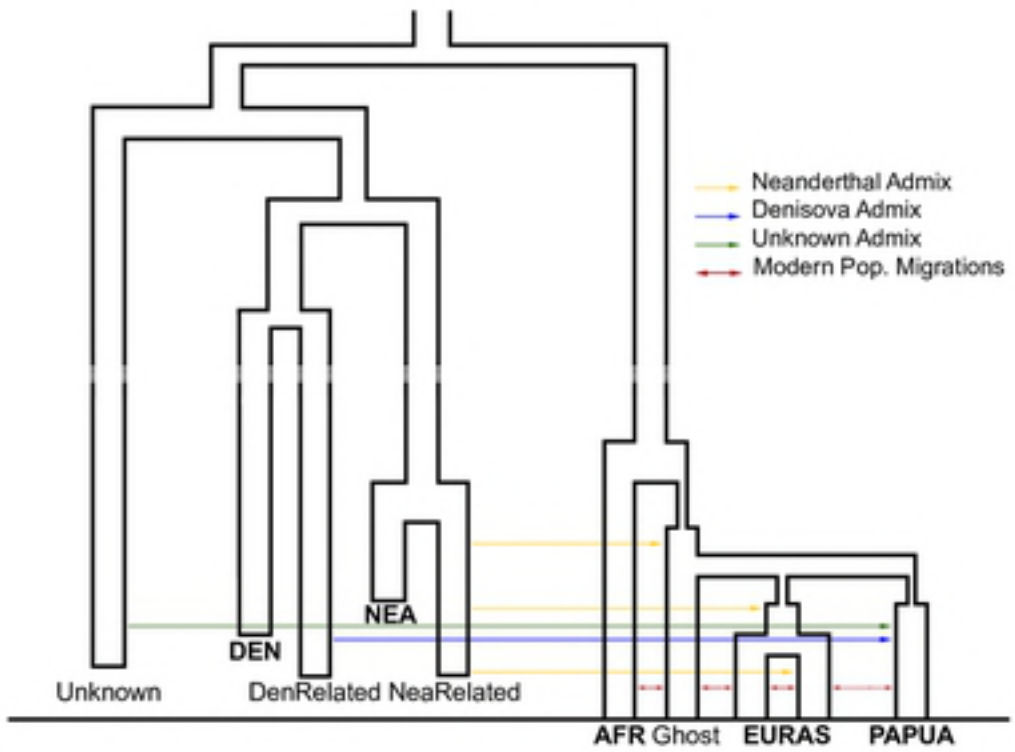
Single Dispersal Model
Neanderthal Admix
Denisova Admix
Unknown Admix
Modern Pop. Migrations
NEA
DEN
Unknown
DenRelated
NeaRelated
AFR
Ghost
EURAS
PAPUA

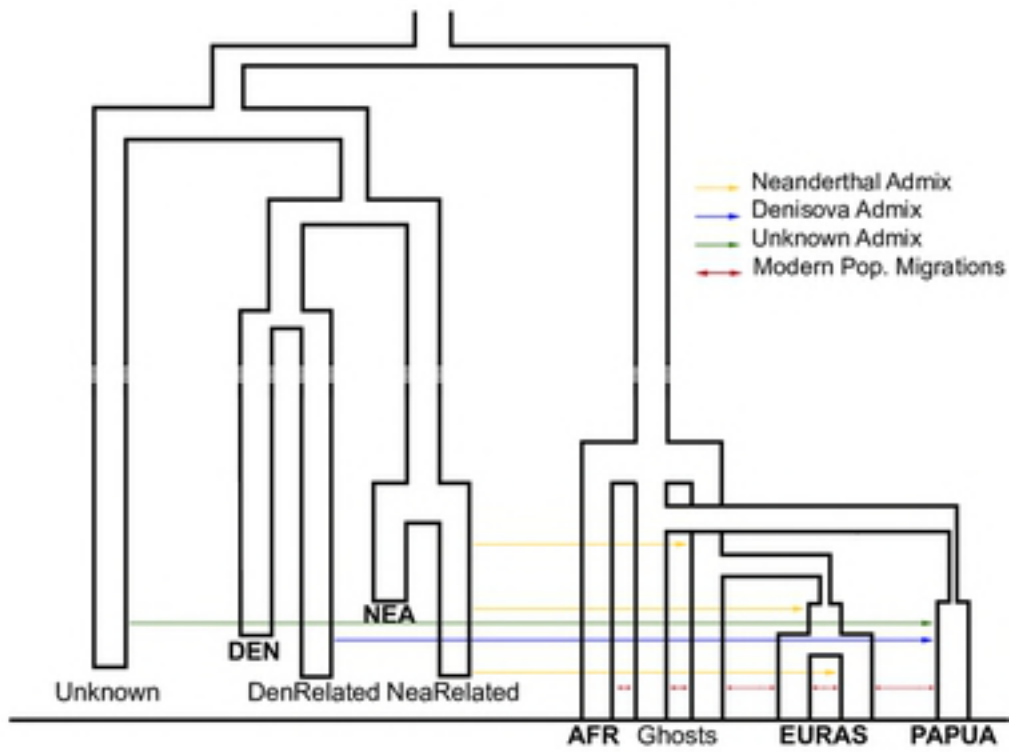
Multiple Dispersal Model
Neanderthal Admix
Denisova Admix
Unknown Admix
Modern Pop. Migrations
NEA
DEN
Unknown
DenRelated
NeaRelated
AFR
Ghosts
EURAS
PAPUA

B

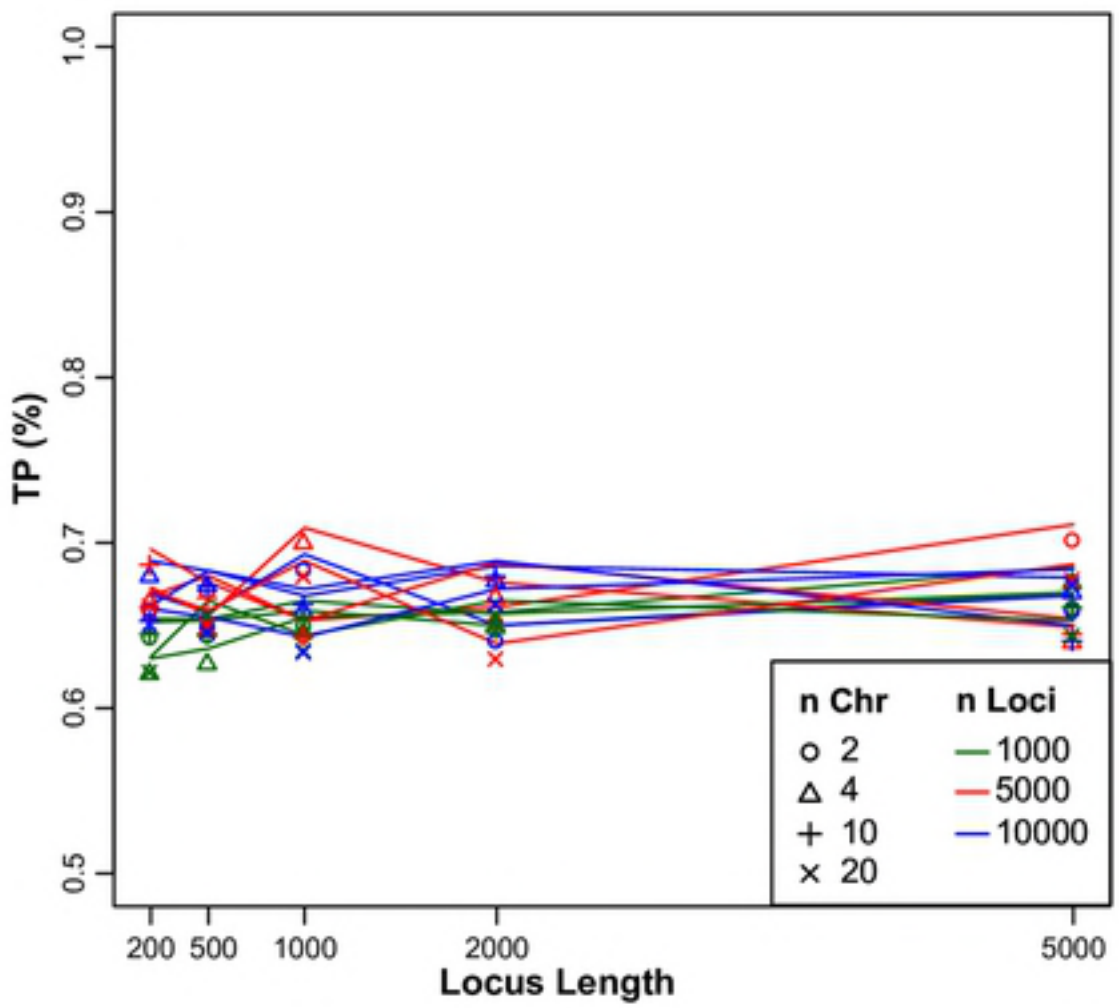
TP (%)
1.0
0.9
0.8
0.7
0.6
0.5
200
500
1000
2000
5000
Locus Length
n Chr
2
4
10
20
n Loci
1000
5000
10000

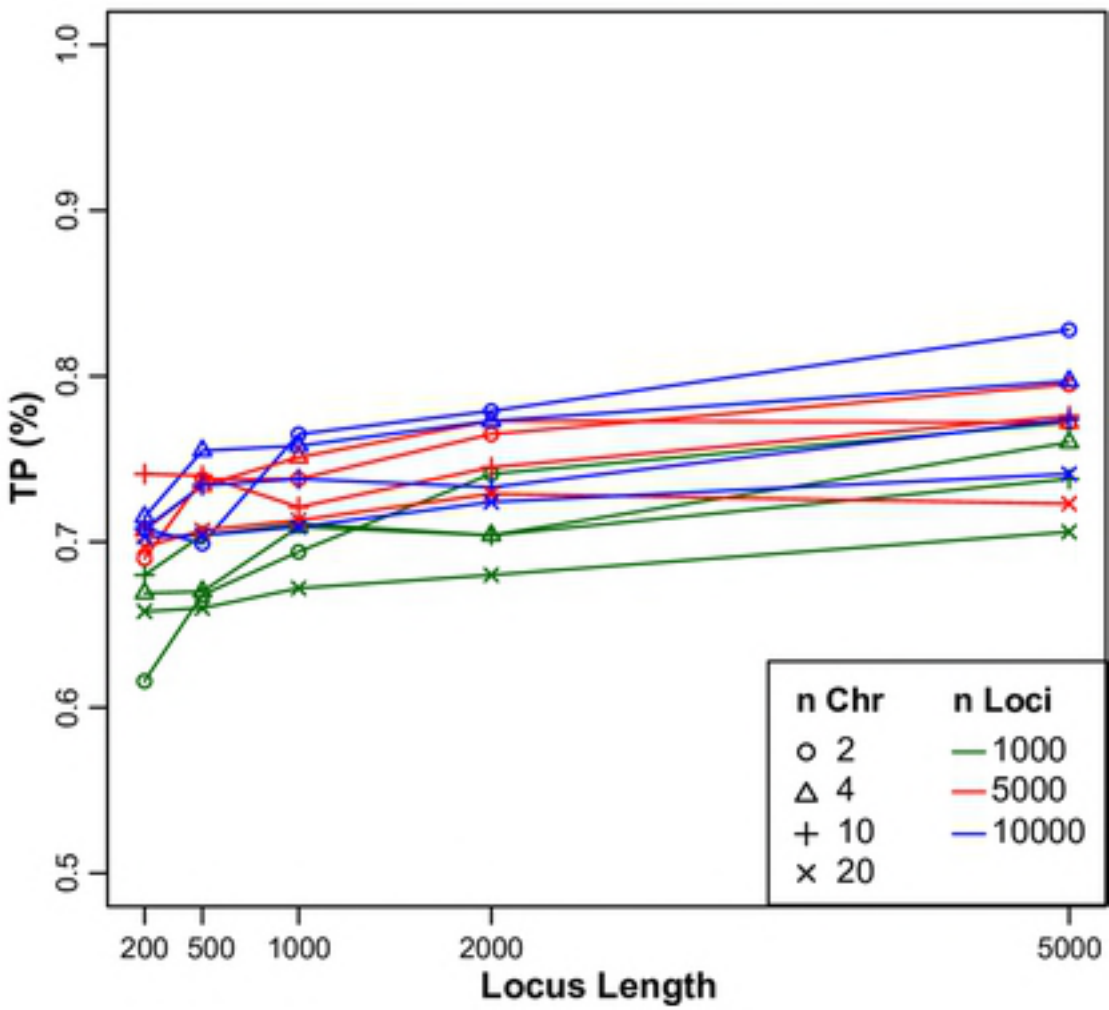
TP (%)
1.0
0.9
0.8
0.7
0.6
0.5
200
500
1000
2000
5000
Locus Length
n Chr
2
4
10
20
n Loci
1000
5000
10000

Figure 3

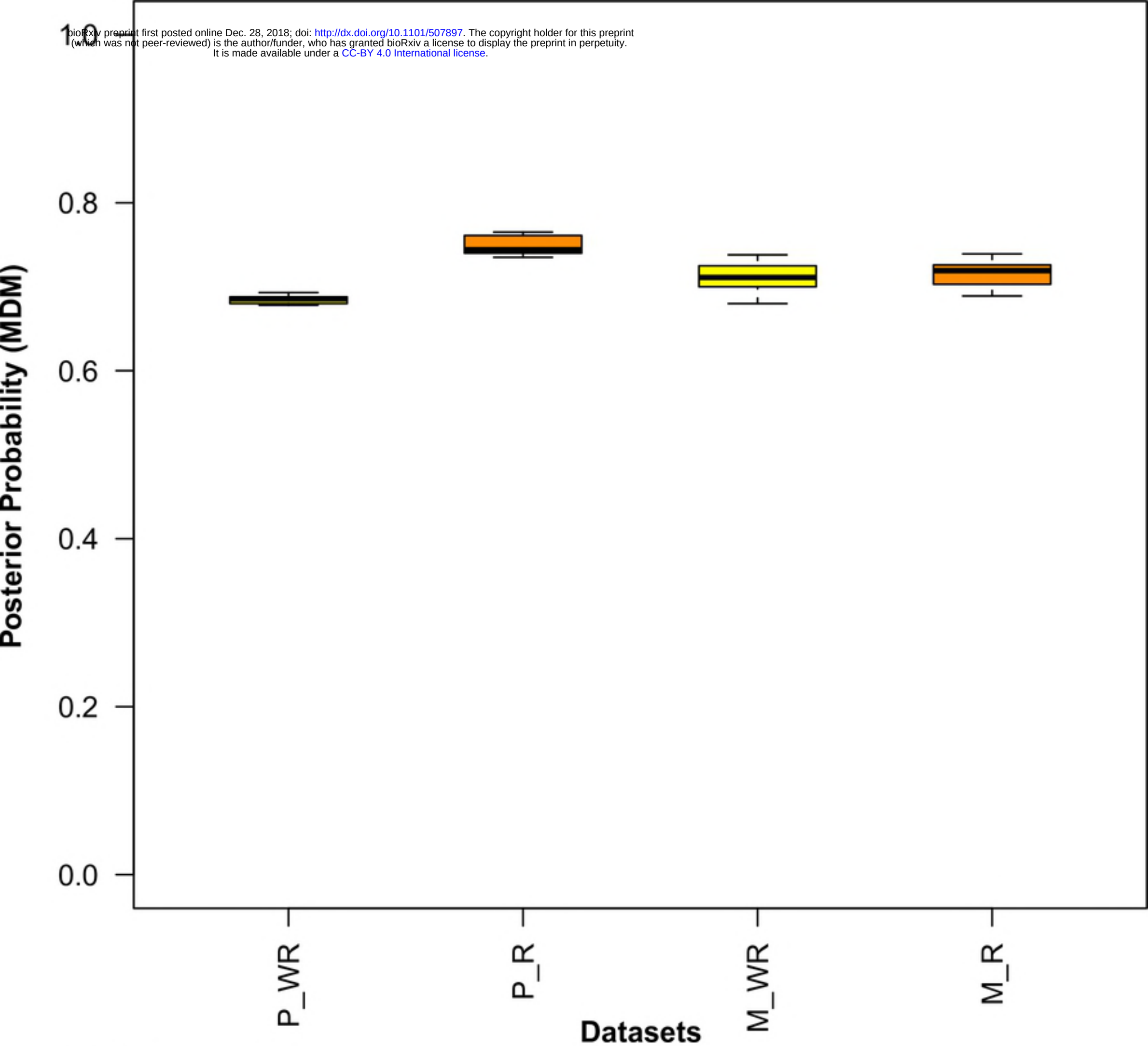


Figure 4